Microfluidics and Nanofluidics manuscript No.
(will be inserted by the editor)

Thermocapillary actuation of droplet in a planar microchannel

Zhenjun Jiao, Xiaoyang Huang, Nam-Trung Nguyen · Patrick Abgrall

Received: date / Revised version: date

The modified parts are highlighted in yellow.

School of Mechanical and Aerospace Engineering, Nanyang Technological University, 50 Nanyang Avenue, Singapore 639798

Abstract A study on thermocapillary actuation of liquid droplet in a planar microchannel has been carried out by both theoretical modeling and experimental characterization. The driving temperature gradients are provided by four heaters at the channel boundaries. In the modeling, the temperature distributions corresponding to transient actuation are calculated, and are coupled to the droplet through the surface tensions which drive the droplet to move inside the channel. The droplet trajectories and final positions are predicted, and are compared with the experimental observations, in which a silicon oil droplet was actuated inside a 10 mm×10 mm planar channel with four heater fabricated on the substrate plate. The results show that the droplet can be positioned anywhere in the channel, determined by a heating code related to the heating strengths. Qualitative agreement between the modeling results and experimental data, in terms of temperature distributions, droplet trajectories and positions, has been obtained.

1 Introduction

With the growing importance of biological science research in micro-scale, droplet-based microfluidics has been emerged as an alternative tool for bio-chemical analysis. Microdroplets can work as carriers for the reactant transport in a lab on a chip (LOC). The emerging field of droplet-based microfluidics leads to the need of effective manipulations of individual droplet in microscale [1]. Most of the LOCs use one-dimensional (1-D) continuous-flow platforms based on microchannels, where the active control of microdroplets can be achieved by pressure differences [2], thermocapillary forces [3] and other forces. In contrast to 1-D droplet-based microfluidic devices, a two dimen-

sional (2-D) droplet-based microfluidic device handles droplets individually with more flexibilities. The actuation may be achieved by chemical or thermal gradients [4], surface acoustic waves [5], electric fields [7], and magnetic fields [6]. Two-dimensional manipulation of droplets by thermal gradient actuation was reported by Darhuber et al. [8][9]. They designed a microfluidic device for the actuation of liquid droplets or continuous streams on a solid surface by means of integrated micro-heater arrays. The micro-heaters provided control of the surface temperature distribution with high spatial resolutions. In combination with chemical surface patterning, the device can be used as a logistic platform for the parallel and automated routing, mixing and reacting of a multitude of liquid samples. In their work, a complex programmable multi-heaters array design was used to achieve the motion control to the droplet. The similar control can be obtained by using boundary-heaters with programmable heating schemes [10][11][12][13]. In these studies, 1-D simulations and experiments were conducted on the dynamics of a liquid plug actuated between two heaters in a capillary. The actuation concept allowed both transient and reciprocating motions. In the present paper, the 1-D model for the capillary tube is extended to a planar microchannel. A liquid droplet is positioned inside the planar channel formed between two parallel glass plates. Four integrated heaters are positioned at the four edges of a plate and form a square area. The square area is considered to be much larger than the droplet size. Temperature distributions in the square region are realized spatially with four controllable heating boundary conditions. Through the coupling between the temperature field and the surface tension, the droplet motion and position are under control. It is to demonstrate that a complete manipulation of the droplet in a region can be achieved by various heating conditions at the boundaries.

2 Modeling of temperature distribution

Figure 1 shows the concept of thermocapillary actuation of a single droplet in a planar microchannel formed between two parallel plates. The gap between the two plates is h_g. Four heaters are located at the boundaries of the bottom plate. In order to simplify the model, a square region is considered in the present study. The temperature distribution induced by the boundary heating on the substrate surface can be described by the following governing equation:

$$\frac{\partial \theta}{\partial t} = \alpha\left(\frac{\partial^2 \theta}{\partial^2 x} + \frac{\partial^2 \theta}{\partial^2 y}\right) - \frac{h}{H\rho c}\theta \tag{1}$$

where θ is the temperature difference relative to the environmental temperature, H is the thickness of the substrate plane, α, ρ, h and c are the thermal diffusivity, density, convection coefficient and specific heat capacity of the substrate material, respectively. Heat radiation is neglected in this model because of the relatively low temperature of the substrate surface. The boundary conditions are:

$$\begin{cases} \frac{\partial \theta}{\partial x}|_{x=0} = -f_1 \frac{q_0^{''}}{k} \\ \frac{\partial \theta}{\partial x}|_{x=a} = f_2 \frac{q_0^{''}}{k} \end{cases}, \quad \begin{cases} \frac{\partial \theta}{\partial y}|_{y=0} = -f_3 \frac{q_0^{''}}{k} \\ \frac{d\theta}{\partial y}|_{y=a} = f_4 \frac{q_0^{''}}{k} \end{cases} \tag{2}$$

where $q_0^{''}$ is the maximum heat flux that can be supplied by individual heater, k is the conductivity of the substrate material and a is the length of the square region edge. The strength factors f_1, f_2, f_3 and f_4 control the heating operation. The factors have values betweem 0 and 1, corresponding to the minimum and the maximum heat flux of the four heaters respectively. By introducing the dimensionless variables $\theta^* = \theta k/(q_0^{''} a), x^* = x/a, t^* = t/(a^2/\alpha)$ and $\xi = ha^2/Hk$ in eqs. (1) and (2), we have the

dimensionless heat transfer equation and boundary conditions:

$$\begin{aligned}
&\frac{\partial \theta^*}{\partial t^*} = (\frac{\partial^2 \theta^*}{\partial^2 x^*} + \frac{\partial^2 \theta^*}{\partial^2 y^*}) - \xi\theta^* \\
&\begin{cases} \frac{\partial \theta^*}{\partial x^*}|_{x^*=0} = -f_1 \\ \frac{\partial \theta^*}{\partial x^*}|_{x^*=1} = f_2 \end{cases}, \begin{cases} \frac{\partial \theta^*}{\partial y^*}|_{y^*=0} = -f_3 \\ \frac{\partial \theta^*}{\partial y^*}|_{y^*=1} = f_4 \end{cases}
\end{aligned} \tag{3}$$

In order to homogenize the boundary conditions, an auxiliary function is introduced,

$$\psi(x^*, y^*) = -f_1 x^* + \frac{x^{*2}}{2}(f_1 + f_2) - f_3 y^* + \frac{y^{*2}}{2}(f_3 + f_4) \tag{4}$$

such that

$$\begin{cases} \frac{\partial \psi}{\partial x^*}|_{x^*=0} = -f_1 \\ \frac{\partial \psi}{\partial x^*}|_{x^*=1} = f_2 \end{cases}, \begin{cases} \frac{\partial \psi}{\partial y^*}|_{y^*=0} = -f_3 \\ \frac{\partial \psi}{\partial y^*}|_{y^*=1} = f_4 \end{cases} \tag{5}$$

By setting

$$\theta^*(x^*, y^*, t^*) = g(x^*, y^*, t^*) + \psi(x^*, y^*) \tag{6}$$

and substituting equation (6) into equation (3), we obtain

$$\frac{dg}{dt^*} = (\frac{d^2 g}{d^2 x^*} + \frac{d^2 g}{d^2 y^*}) - \xi g + (f_1 + f_2 + f_3 + f_4) - \xi\psi \tag{7}$$

and

$$\begin{cases} \frac{\partial g}{\partial x^*}|_{x^*=0} = 0 \\ \frac{\partial g}{\partial x^*}|_{x^*=1} = 0 \end{cases}, \begin{cases} \frac{\partial g}{\partial y^*}|_{y^*=0} = 0 \\ \frac{\partial g}{\partial y^*}|_{y^*=1} = 0 \end{cases} \tag{8}$$

Function $g(t^*, x^*, y^*)$ in equation (7) is solved by the Fourier series which meet the boundary condition (8). Let

$$\begin{aligned}
g = {} & g_{00}(t^*) + \sum_{m=1}^{\infty} g_{m0}(t^*)\cos(m\pi x^*) + \sum_{n=1}^{\infty} g_{0n}(t^*)\cos(n\pi y^*) \\
& + \sum_{m=1}^{\infty}\sum_{n=1}^{\infty} g_{mn}(t^*)\cos(m\pi x^*)\cos(n\pi y^*)
\end{aligned} \tag{9}$$

where g_{00}, g_{m0}, g_{0n} and g_{mn} are the coefficients to be determined, and

$$\begin{aligned}
\psi(x^*, y^*) = {} & \psi_{00} + \sum_{m=1}^{\infty} \psi_{m0}\cos(m\pi x^*) + \sum_{n=1}^{\infty} \psi_{0n}\cos(n\pi y^*) \\
& + \sum_{m=1}^{\infty}\sum_{n=1}^{\infty} \psi_{mn}\cos(m\pi x^*)\cos(n\pi y^*)
\end{aligned} \tag{10}$$

where

$$\begin{cases} \psi_{00} = \int_0^1 \int_0^1 \psi \mathrm{d}x^* \mathrm{d}y^* \\ \psi_{m0} = 2\int_0^1 \int_0^1 \psi \cos(m\pi x^*) \mathrm{d}x^* \mathrm{d}y^* \\ \psi_{0n} = 2\int_0^1 \int_0^1 \psi \cos(n\pi y^*) \mathrm{d}x^* \mathrm{d}y^* \\ \psi_{mn} = 4\int_0^1 \int_0^1 \psi \cos(m\pi x^*) \cos(n\pi y^*) \mathrm{d}x^* \mathrm{d}y^* \end{cases} \tag{11}$$

Substituting equations (9)-(11) into (7), taking the initial condition $\theta(x^*, y^*, 0) = 0$, the final result for the temperature is obtained as:

$$\begin{aligned} &\theta^*(x^*, y^*, t^*) = g(x^*, y^*, t^*) + \psi(x^*, y^*) \\ &= g_{00}(t^*) + \sum_{m=1}^{\infty} g_{m0}(t^*) \cos(m\pi x^*) + \sum_{n=1}^{\infty} g_{0n}(t^*) \cos(n\pi y^*) \\ &-f_1 x^* + \frac{x^{*2}}{2}(f_1 + f_2) - f_3 y^* + \frac{y^{*2}}{2}(f_3 + f_4) \end{aligned} \tag{12}$$

where

$$\begin{cases} g_{00} = d_{00} - \psi_{00} + d_{00} e^{-\xi t^*} \\ g_{m0} = \frac{\xi}{\beta}\psi_{m0} + d_{m0} e^{-\beta t^*} \\ g_{0n} = \frac{\xi}{\gamma}\psi_{0n} + d_{0n} e^{-\gamma t^*} \end{cases}, \begin{cases} d_{00} = -\frac{1}{\xi}(f_1 + f_2 + f_3 + f_4) \\ d_{m0} = -\left(1 + \frac{\xi}{\beta}\right)\psi_{m0} \\ d_{0n} = -\left(1 + \frac{\xi}{\gamma}\right)\psi_{0n} \end{cases} \tag{13}$$

and $\beta = (m\pi)^2 + \xi$, $\gamma = (n\pi)^2 + \xi$. The cross terms, $\cos(m\pi x^*)\cos(n\pi y^*)$, do not appear in the solution because $\psi_{mn} = g_{mn} = 0$.

3 Coupling of the temperature field with the droplet motion

The temperature distributions in the channel are coupled to the droplet motion through surface tensions. The unbalanced surface tensions on the droplet, due to the temperature gradients, drive the droplet moving inside the channel. The surface tension σ of the liquid depends on the temperature. For a small temperature range, a linear relation can be assumed:

$$\sigma_{\mathrm{lg}}(\theta) = \sigma_{\mathrm{lg0}} - \varepsilon(\theta - \theta_0) \tag{14}$$

where $\sigma_{\mathrm{lg}0}$ is the liquid-gas surface tension at the reference temperature θ_0 and ε is the temperature coefficient of surface tension. The temperature field resulting from equation (1) is in turn a function of the position (x, y). Assuming a weak thermal interaction between the droplet and the substrate surface, the surface tension can be described as a function of the position (x, y) through the temperature distributions:

$$\sigma_{\mathrm{lg}}(\theta) = f[\theta(x, y)] = \sigma_{\mathrm{lg}}(x, y) \tag{15}$$

Since the droplet diameter $2R$ is normally less than the Laplace length κ^{-1} ($\kappa^2 = \rho g/\sigma_{\mathrm{lg}}$), the droplet profile can be assumed to be circular, the curvature radius be constant and the dynamic contact angle be uniform along the contact line. For flat structures the dominant viscous dissipation occurs in the bulk, and the dissipation at the solid-liquid-gas contact line is negligible. With the lubrication approximation, the viscous drag force generated within the liquid is [14]

$$\begin{cases} D_x = 3\mu u \displaystyle\int_{\mathrm{M}}^{\mathrm{N}} \frac{\mathrm{d}x}{\lambda(x)} = \frac{6\mu u R}{h_g} \\ D_y = 3\mu v \displaystyle\int_{\mathrm{P}}^{\mathrm{Q}} \frac{\mathrm{d}y}{\lambda(y)} = \frac{6\mu v R}{h_g} \end{cases} \tag{16}$$

where $\lambda(x)$ is the droplet height profile function, u, v are the velocity magnitudes on x and y directions respectively, μ is the liquid viscosity, R is the the droplet base radius, and h_g is the channel height. The liquid viscosity, based on the previous work of Yarin, is dependent on temperature at the droplet center [15],

$$\mu = \mu_0 \exp\left[3.8 T_b \left(\frac{1}{T_{\mathrm{center}}} - \frac{1}{T_0}\right)\right] \tag{17}$$

where μ_0 is the viscosity at a reference temperature T_0(normally 293K), and T_b is the liquid boiling temperature. In order to make the droplet evaporate with an imperceptible amount and to make hysteretic effects not prominent, silicone oil was chosen to be the droplet liquid. In this case, the capillary number is $Ca = \dfrac{\mu|\vec{U}|}{\sigma_{\mathrm{lg}}} < 1 \times 10^{-3}$ when

the droplet velocity magnitude $|\overrightarrow{U}|$ is less then 1 mm/s, where $\overrightarrow{U} = u\hat{x} + v\hat{y}$ is the droplet velocity. The low capillary number ensures that the moving droplet consistently has a circular shape. For simplification, the dynamic contact angles are assumed to be constant. The circular shape is divided into n finite sections, the resultant force on both x, and y directions can be calculated by combining all the surface tension forces acting on individual sector,

$$\begin{cases} F_x = 2\sum_{i=1}^{n} \frac{2\pi R}{n} \cos\left[\frac{(2i+1)\pi}{n}\right] \sigma_{\mathrm{lg}}(x_i, y_i) \\ F_y = 2\sum_{i=1}^{n} \frac{2\pi R}{n} \sin\left[\frac{(2i+1)\pi}{n}\right] \sigma_{\mathrm{lg}}(x_i, y_i) \end{cases} \tag{18}$$

where $\sigma(x_i, y_i) = \sigma\left\{x_0 + R\cos\left[\frac{\pi(2i+1)}{n}\right], y_0 + R\sin\left[\frac{\pi(2i+1)}{n}\right]\right\}$, (x_0, y_0) is the droplet initial center point position. A larger n leads to a more accurate result, and we set $n = 8$ in this study. The velocity $\overrightarrow{U}$ can be determined by the force balance between the acceleration, friction and thermocapillary force, i.e.,

$$\begin{cases} \rho V \frac{\mathrm{d}u}{\mathrm{d}t} = -\frac{6\mu R}{h_g} u + F_x \\ \rho V \frac{\mathrm{d}v}{\mathrm{d}t} = -\frac{6\mu R}{h_g} v + F_y \end{cases} \tag{19}$$

V is the volume of the droplet($V \approx \pi R^2 h_g$). The dynamic contact angle along the contact line is assumed to be the same as the static contact angle of approximately 10°. By setting $A = \frac{6\mu R}{\rho V h}$, $B_x = -\frac{F_x}{\rho V}$ and $B_y = -\frac{F_y}{\rho V}$, the velocity of the droplet can be solved as

$$\begin{cases} u = -\frac{B_x}{A} + \frac{B_x}{A} e^{-At} \\ v = -\frac{B_y}{A} + \frac{B_y}{A} e^{-At} \end{cases} \tag{20}$$

4 Experiments setup and materials

The experimental setup is illustrated in Figure 2. The planar channel was formed between two parallel glass plates. The gap between the parallel plates was 0.5 mm. Four

Table 1 Physical properties of silicone oil.[8]

Properties	Silicone oil
Density ρ in kg/m^3	930
Surface tension (293K) $\sigma_{\mathrm{lg}0}$ in mN/m	20.3
Temperature coefficient of surface tension ε in mN/m·K	0.06
Kinematic viscosity (293K) ν_0 in m^2/s	10^{-5}
Boiling point T_b in K	413

micro heaters, made of thin-film titanium and platinum, were sputtered and structured on the glass wafer along four sides of a 10 mm×10 mm square region. The droplet was actuated within this square region. In the experiments, the maximum heating power was kept at 0.5 W for all heaters. An customized circuit was used to control individual heaters according to the required heating code. The control signal can also be used to trigger a CCD camera for capturing the droplet motion images. The CCD camera was operated at rate of two frames per second throughout the experiments. The resolution of the camera was 640 pixels × 480 pixels. A thermal tracer camera (NEC TH9100PMVI) was used for the measurement of the temperature distribution. Silicone oils PDMS (polydimethylsiloxane, Sigma Aldrich) of viscosity 10 cSt was used in the experiments as the working liquid for the droplets, and the droplet radius was kept at 0.5-0.7 mm. The droplet was injected into the planar channel by a precise syringe. The physical properties of silicone oil are listed in Table 1.

5 Results and discussions

5.1 Simulation results

In the transient actuation of our present study, the heaters are switched on with constant heat fluxes. Under this operation mode, the temperature field is established in a transient time period and the final temperature distribution will depend on a heating code formed by the combination (f_1, f_2, f_3, f_4). Figure 3 shows the temperature distributions at different time instances after switching on the heaters. In this case, the four heaters have an equal heat flux and the corresponding heating code is (1,1,1,1). The temperature increases from the heater sides and stabilizes into a symmetric distribution with the lowest temperature at the center of the square plate. The motion of a droplet driven by this heating process is plotted in Figure 4. The droplet is moving from its initial location towards the center and stays there, as illustrated in Figure 4(a). The dimensionless displacement and dimensionless velocity(normalized by α/a) of the droplet, together with the dimensionless temperature gradient magnitude at the droplet center position, are shown in Figures 4(b), 4(c) and 4(d). The droplet is accelerated by a large temperature gradient following activation of the heaters, reaches a maximum velocity before slowing down, and finally stops at the channel center $(0.5, 0.5)$, where the temperature gradient is zero.

The final temperature distributions associated with four different heating codes are plotted in Figure 5, among them three are not symmetric. Figure 6 shows the trajectories of the droplet corresponding to the different heating codes and temperature distributions shown in Figure 5. Testing with different initial positions of the droplet, the results show that the final positions are independent of the initial locations. This feature could be used for mixing of droplets which may contain different samples and

are initially positioned at different locations on the platform. By comparing to the dimensionless temperature fields in Figure 5, the end position of the droplet is seen to be the lowest temperature point in each case, where the temperature gradient is zero and so is the actuation force. Once the droplet reaches this point, it is trapped there. Theoretically, the droplet can be driven to any position from any initial position by using different heating codes. Lowering down the heat flux of any heater, relative to others, will lead to the end position being closer to it.

5.2 Experimental characterization

The experimental characterizations of the droplet actuated in the planar channel were conducted to verify the simulation results, and also to demonstrate that the concept is achievable. Figure 7 shows the transient temperature distributions captured by the thermal tracer camera at different time instances after activating the four heaters with the same power. This case corresponds to a heating code of (1,1,1,1). Comparing with the predicted temperature distributions shown in Figure 3, the experimental results agree relatively well with the modeling results, except the low temperatures at the four corners. This is because the nonuniform heat flux along the individual micro heater, especially at the corners where two heaters are not joined as the boundary conditions assumed in the simulation. Under the symmetric actuation $(f_1, f_2, f_3, f_4) = (1, 1, 1, 1)$, Figure 8(a) shows selected images of a silicon oil droplet moving from a corner of the planar channel towards the center at different time instances. The process and trajectories are similar to that predicted by the simulation. Figures 8(b) and 8(c) show the displacement and velocity of the droplet center point versus time evaluated from the recorded images. The velocity was calculated by using the results of two subsequent

frames to get the displacements Δx and Δy, so that $u = \Delta x/\Delta t$, $v = \Delta y/\Delta t$, and $\Delta t = 0.5$ second determined by the frame rate. The velocity is therefore obtained as $\sqrt{u^2 + v^2}$. The results show clearly that the droplet is initially accelerated, reaching to a maximum velocity before slowing down, and is finally trapped at the center of the square region, where the temperature is the lowest. The results qualitatively agree with the predicted moving tracks and velocities which are also plotted in Figures 8(b) and 8(c). In order to further verify the modeling results, the silicon droplet was actuated with two more heating codes, $(f_1, f_2, f_3, f_4) = (1, 0.3, 1, 0.3)$ and $(f_1, f_2, f_3, f_4) = (1, 0.3, 0.3, 1)$ respectively. The results are shown in Figure 9, which are selected images of the droplet motion at different time instances. It is seen that, in case of $(1, 0.3, 1, 0.3)$, the droplet has been driven from the lower-left corner to the upper-right corner, as shown in Figure 9(a). While in the case of $(1, 0.3, 0.3, 1)$, the droplet was initially driven to the channel center, then it turned to the right and finally stoped at the lower-right corner, as depicted in Figure 9(b). The experimental observations on both cases agree with the predicted results described in Figures 6(d) and 6(c).

6 Conclusion

The thermocapillary actuation of a silicon oil droplet in a planar microchannel has been investigated by simulations and verified by experiments. The heaters are located at the four sides of the channel and the actuation is achieved by controlling the heating strength factors. Qualitative agreement has been obtained between the modeling results and experimental characterizations, in terms of temperature distributions, droplet trajectories, positions and velocities. The results show that the droplet can be manipulated with a great flexibility in terms of positions and trajectories. The droplet can

be positioned anywhere in the channel, determined by the heating codes according to the strength of individual heater. The actuation concepts reported in this paper would have potential applications in droplet-based microfluidics, such as concurrent mixing and moving of biological and chemical samples contained in the liquid in planar channels. The medium for the samples can be silicone oil [16], which has been used in the present study. Due to evaporation and the small temperature dependency of surface tension, aqueous solutions may not be suitable for thermocapillary actuation. In this case, the aqueous solution can be encapsulated by bigger oil droplets [12].

Acknowledgement

The authors would like to acknowledge the financial support provided by the Academic Research Fund of the Ministry of Education Singapore (grant no RG26/06).

References

1. Song H, Chen DL, Ismagilov RF (2006) Reactions in droplets in microfluidic channels. Angew. Chem. Int. Ed. 45:7336-7356.
2. Link D, Anna SL, Weitz D, Stone HA (2004) Geometric mediated breakup of drops in microfluidic devices. Physical Review Letters 92:054503.
3. Ting TH, Yap YF, Nguyen NT, Wong TN, Chai JCK, Yobas L (2006) Thermally mediated breakup of drops in microchannels. Applied Physics Letter 89:234101.
4. Brochard F (1988) Motions of droplets on solid surfaces induced by chemical or thermal gradients. Langmuir 5:432-438.
5. Strobll CJ, Rathgeber A, Wixforth A, Gauer C, Scriba J (2002) Planar microfluidic processors. Proceedings of the IEEE Ultrasonics Symposium 1, 255-258.
6. Nguyen NT, Beyzavi A, Ng KM, Huang XY (2007) Kinematics and deformation of ferrofluid droplets under magnetic actuation. Microfluidics and Nanofluidics 3:571-579.

7. Velev OD, Prevo BG, Bhatt KH (2003) On-chip manipulation of free droplets. Nature 426:515-516.
8. Darhuber AA, Davis JM, Troian SM, Reisner WW (2003) Thermocapillary actuation of liquid flow on chemically patterned surfaces. Phys. Fluids 15:1295-304.
9. Darhuber AA, Valentino JP, Troian SM, Wagner S (2003) Thermocapillary actuation of droplets on chemically patterned surfaces by programmable microheater arrays. J. Microelectromech. Syst 12:873-879.
10. Nguyen NT and Huang XY (2005), Thermocapillary effect of a liquid plug in transient temperature field. Japanese Journal of Applied Physics 94:1139-1142.
11. Jiao ZJ, Nguyen NT, Huang XY, Ang AZ (2007), Reciprocating thermocapillary plug motion in an externally heated capillary. Microfluidics and Nanofluidics 3:39-46.
12. Jiao ZJ, Nguyen NT, Huang XY (2007) Thermocapillary actuation of a water droplet encapsulated in an oil plug, Journal of Micromechanics and Microengineering 17:1843-1852.
13. Jiao ZJ, Nguyen NT, Huang XY (2007) Thermocapillary actuation of liquid plugs using a heater array, Sensors and Actuators A, in doi:10.1016/j.sna.2007.06.025.
14. Daniel S, Chaudhury MK (2002) Rectified motion of liquid drops on gradient surfaces induced by vibration. Langmuir 18:3404-3407.
15. Yarin AL, Liu WX, Reneker DH (2002) Motion of droplets along thin fibers with temperature gradient. Journal of Applied Physics 91:4751.
16. Su F, Chakrabarty K, Fair RB (2006) Microfluidics-based biochips: Technology issues, implementation platforms, and design-automation challenges. IEEE Transactions on Computer-Aided Design of Integrated Circuits and Systems 25:211-223 .

List of figures

– Figure 9: Images of the silicon oil droplet at different time instances. (a) The heating code is $(f_1, f_2, f_3, f_4) = (1, 0.3, 1, 0.3)$; (b) The heating code is $(f_1, f_2, f_3, f_4) = (1, 0.3, 0.3, 1)$.

Fig. 1 Schematic illustration of the actuation of droplet in a planar channel. (a)The channel and heaters. (b)The droplet configuration.

Fig. 2 Experimental setup.

Fig. 3 The transient temperature distributions at different time instances: (a) $t^* = 0.0075$; (b) $t^* = 0.075$; (c) $t^* = 0.375$; (d) $t^* = 0.75$. The heating code is $(f_1, f_2, f_3, f_4) = (1, 1, 1, 1)$.

Fig. 4 (a) The trajectory of the droplet with the heating code $(f_1, f_2, f_3, f_4) = (1, 1, 1, 1)$. (b) Position of the droplet versus time in both x and y directions. (c) Velocity magnitude of the droplet versus time. (d) Temperature gradient magnitude at the droplet center against time.

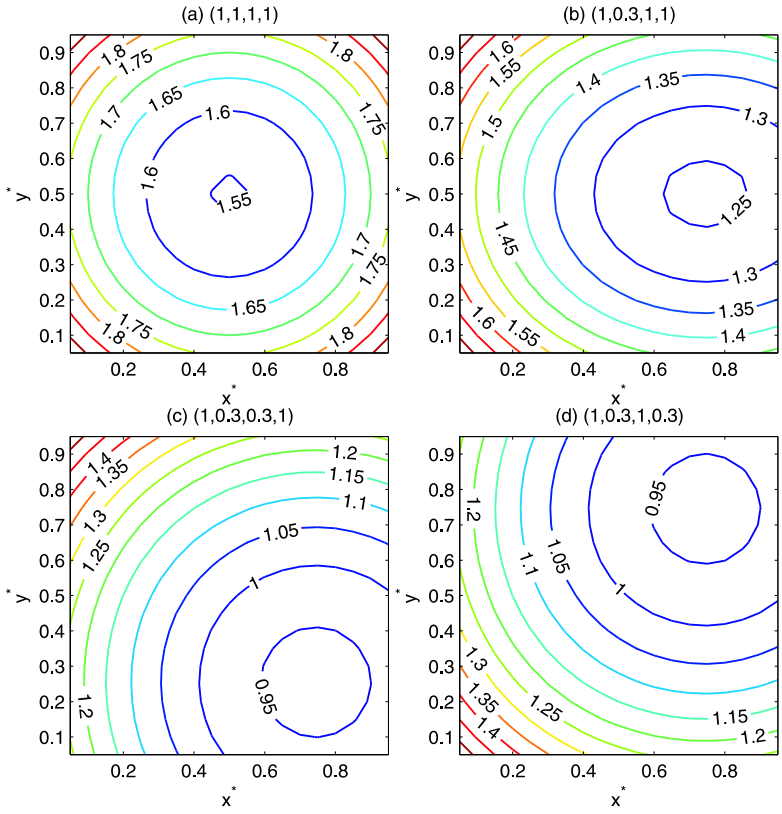

Fig. 5 The final temperature distributions generated by different heating codes: (a) $(f_1, f_2, f_3, f_4) = (1, 1, 1, 1)$, (b) $(f_1, f_2, f_3, f_4) = (1, 0.3, 1, 1)$, (c) $(f_1, f_2, f_3, f_4) = (1, 0.3, 0.3, 1)$, (d) $(f_1, f_2, f_3, f_4) = (1, 0.3, 1, 0.3)$.

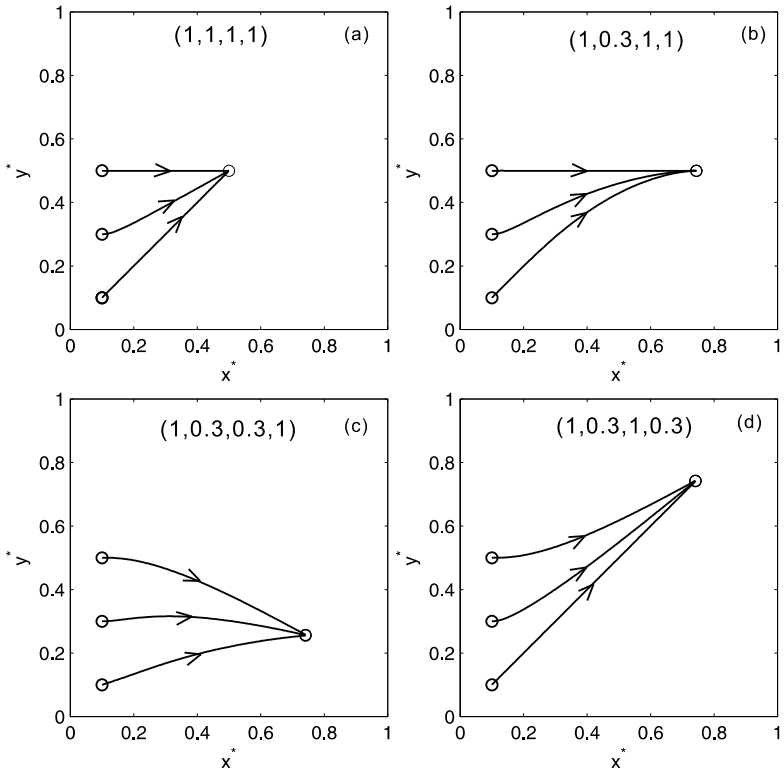

Fig. 6 (a)-(d) The corresponding tracks of the droplet movements, with different initial positions, driven by the transient temperature fields described in Figures 5(a)-(d).

Fig. 7 The experimental results of transient temperature distributions at different time: (a) $t = 1s$; (b) $t = 5s$; (c) $t = 10s$; (d) $t = 50s$. The heating code is $(f_1, f_2, f_3, f_4) = (1, 1, 1, 1)$.

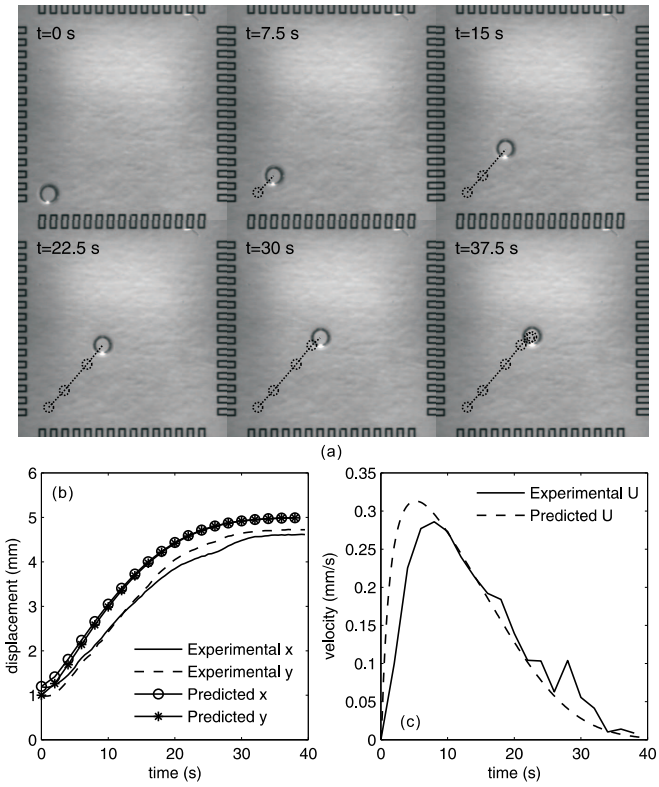

Fig. 8 (a) Images of the silicon oil droplet at different time instances. (b) The positions of the droplet center versus time. (c) Variations of velocity of the droplet center versus time. The heating code is $(f_1, f_2, f_3, f_4) = (1, 1, 1, 1)$.

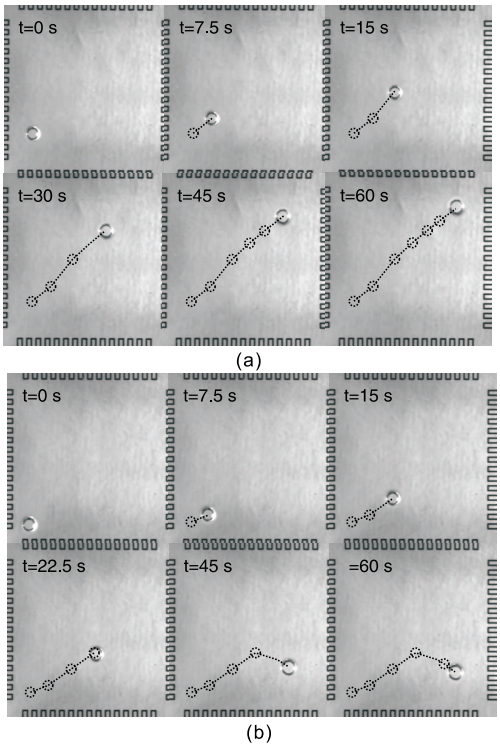

Fig. 9 Images of the silicon oil droplet at different time instances. (a) The heating code is $(f_1, f_2, f_3, f_4) = (1, 0.3, 1, 0.3)$; (b) The heating code is $(f_1, f_2, f_3, f_4) = (1, 0.3, 0.3, 1)$.